European Journal of Pharmacology 1003 (2025) 177999

Contents lists available at ScienceDirect

European Journal of Pharmacology

journal homepage: www.elsevier.com/locate/ejphar

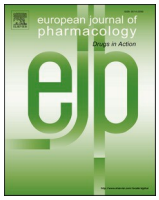

Graphitic carbon nitride nanoparticle: g-C_3N_4 synthesis, characterization, and its biological activity against glioblastoma

Anxo Vila Alonso [a,b], Akshaya Murugesan [a,b], Rituporn Gogoi [c], Sureka Chandrabose [d], Kasim S. Abass [e], Vipul Sharma [c], Meenakshisundaram Kandhavelu [a,b,*]

[a] Molecular Signaling Group, Faculty of Medicine and Health Technology, Tampere University, Tampere, Finland
[b] BioMeditech and Tays Cancer Center, Tampere University, Hospital, P.O. Box 553, 33101, Tampere, Finland
[c] Department of Mechanical and Materials Engineering, University of Turku, 20014, Turku, Finland
[d] Department of Basic Medical Sciences, College of Medicine, Prince Sattam Bin Abdulaziz, Saudi Arabia
[e] Department of Physiology, Biochemistry, and Pharmacology, College of Veterinary Medicine, University of Kirkuk, Kirkuk, 36001, Iraq

ARTICLE INFO

Keywords:
Graphitic carbon nitride
Glioblastoma
Growth inhibition
Migration
Cell cycle analysis

ABSTRACT

Graphitic carbon nitride, (g-C_3N_4), is a polymeric derived carbon-nitrogen molecule, and its derivatives have found extensive application in biomedicine. Synthetic g-C_3N_4 nanoparticles (GCN-Np) stands out for their anti-cancer activity attributed to their conductivity, strength, chemical and thermal endurance. Here, we investigate the potential mechanism action and efficacy of GCN-Np in glioblastoma cells. The mechanically synthesized g-C3N4 was structurally characterized using Field emission scanning electron microscopy, Fourier transform infrared spectroscopy, UV-Spectroscopy, and X-ray diffraction techniques. The findings revealed that the GCN-Np displayed C=N stretching, C–N, -NH- and -NH_2 functional groups attributed to the graphitic carbon compounds with an average particle size of 300 nm. Cell death analysis indicated that the IC50 concentrations of GCN-Np and TMZ are 4.7 μg/mL and 9.3 μg/mL for LN229, and 15.9961 μg/mL and 16.8 μg/mL for SNB19 GBM cells, respectively. GCN-Np effectively arrested the cell cycle at S phase approximately <50 %, in both GBM cells, thereby preventing the possibility of cell division prior to DNA synthesis. FACS analysis validated the role of GCN-Np and TMZ in eliciting ROS-mediated apoptosis at around 91 % and 93 %, respectively. Finally, the ability of GCN-Np to prevent the migration of GBM cells was observed to be significantly higher than the TMZ. In non-cancerous cells, MEF, GCN-Np demonstrates minimal cytotoxicity, confirming its selective targeting of malignant cells. Overall, the GCN nanoparticles exhibited promising anti-GBM effects with minimal cytotoxicity to non-cancerous MEF cells, suggesting their potential for further therapeutic investigations.

1. Introduction

Graphitic carbon nitride (g-C_3N_4) a graphene-like polymeric substance, possesses exceptional physical and chemical properties with good biocompatibility (Heo et al., 2018; Wang et al., 2021; Zhang et al., 2016). Its broader applications in biomedicine stem from its adjustable solubility, and photoelectric properties, which are not yet sufficiently revealed. The primary characteristic of consideration of this g-C3N4 is the exclusive existence of carbon and nitrogen, which does not influence the biological properties of any molecules (Cheng et al., 2020). Over the past twenty years, novel derivatives of carbon nanostructures including graphitic nitride carbon, graphene, and carbon nanosheets have surfaced as promising candidates for the advancement of biomedical devices for drug delivery (Kim et al., 2024; Maiti et al., 2019).

Cancer is the second most common cause of death worldwide and is estimated to reach approximately 10 million deaths by 2028 (Anandasabapathy et al., 2024). Despite significant advances in cancer treatment, particularly glioblastoma multiforme (GBM), this aggressive malignant brain cancer has a minimal life expectancy of <15 months (Hanif et al., 2017; Louis et al., 2016; Marucci et al., 2011; McKinnon et al., 2021). Currently, the standard treatment for this type of cancer involves a combination of chemotherapy with temozolomide, surgery to remove the tumor, and/or radiotherapy (Yalamarty et al., 2023). However, the use of these drugs is impeded by the development of drug resistance and risk of recurrence. Thus, a new approach necessitates innovative strategies to meet the current clinical need to improve

* Corresponding author. Molecular Signaling Group, Faculty of Medicine and Health Technology, Tampere University, Tampere, Finland
E-mail address: meenakshisundaram.kandhavelu@tuni.fi (M. Kandhavelu).

https://doi.org/10.1016/j.ejphar.2025.177999
Received 14 May 2025; Received in revised form 17 July 2025; Accepted 24 July 2025
Available online 25 July 2025

patient outcomes.

Recent advances in the field of nanotechnology increased the biological application of nanomaterials for cancer therapy. The nanomaterials have smaller dimension ranging from 1 nm to 100 nm, with large surface area, which is the main reason for the different chemical and biological properties (Foo and Fu, 2021; Fu et al., 2014). Nanomaterials are capable of readily passing through membranes and other biological barriers due to their small size, which enables them to be absorbed by living cells and elicit a response therein. Furthermore, nanomaterials have been reported to be reactive and catalytic, capable of inducing cytotoxicity once they have entered the cells. (Akhtar et al., 2015; Anh Tran et al., 2014; Foo and Fu, 2021; Saleem et al., 2018).

In the present work, we have mechanically synthesized and structurally characterized GCN nanoparticles (GCN-Np) through Field emission scanning electron microscopy (FE-SEM), FT-IR, UV-Spectroscopy, and X-ray diffraction techniques. We performed several *in vitro* assays to investigate the cytotoxicity of the GCN-Np against GBM including its potential to arrest the cell cycle and induce apoptosis upon ROS production and change in the mitochondrial membrane potential, ability to prevent the migration of GBM cells. The results were comparable with the conventional drug, TMZ. Overall, the findings could be applied to further comprehend the anti-GBM potential of nanoparticles and its interaction with the GBM cells in comparison with the currently used chemotherapeutic drug, TMZ.

2. Experimental section

2.1. Materials

The material used in this work were, Dulbecco's Modified Eagle Medium (DMEM), fetal bovine serum (FBS), Streptomycin, Penicillin (Sigma-Aldrich, St. Louis, MO, United States); Propidium Iodide, ThermoFisher Scientific, Waltham, MA, USA; Dulbecco's Phosphate buffered saline (D8662, Sigma-Aldritch); Acridine Orange (AO), A6014-10G, Sigma-Aldritch) and Ethidium Bromide (EB); Dimethyl sulfoxide (DMSO); hydrogen peroxide; 2′,7′-dichlorodihydrofluorescein diacetate (H2DCFDA) (Sigma-Aldrich, St. Louis, MO, United States); (5,5,6,6′-tetrachloro-1,1′,3,3′ tetraethylbenzimi-dazoylcarbocyanine iodide) (JC-10 dye) (MAK159-1 KT, Sigma-Aldritch). Dicyandiamide (CAS No. 461-58-5) and Absolute ethanol (EtOH) (CAS No. 64-17-5) were purchased from Sigma-Aldrich, St. Louis, MO, United States and used directly without further treatments or purification.

2.2. Synthesis of graphitic carbon nitride (GCN)

Bulk GCN was synthesized by subjecting 4 g to a furnace temperature at 550 °C for 4 h, with a heating rate of 5 °C/min. The resulting product was pulverized into a fine powder and underwent a secondary heating process at 500 °C (5 °C/min) for 2 h. Upon cooling to ambient temperature, the synthesized GCN was directly utilized for the fabrication of GCN nanoparticles (Alam et al., 2019).

2.3. Synthesis of graphitic carbon nitride (GCN) nanoparticle

To synthesize GCN nanoparticles, 0.5 g of bulk GCN was mechanically pulverized with 1.5 mL of ethanol using an agate mortar and pestle until the solvent evaporated. This process was executed twice to ensure consistent grinding. The resultant material was further dried in a hot air oven at 60 °C for 2 h. The dry powder was then dispersed in 10 mL of ethanol and subjected to sonication for 10 min in a bath sonicator. The suspension was allowed to remain undisturbed overnight to facilitate the sedimentation of the denser GCN particles. Finally, 5 mL of the supernatant containing GCN nanoparticles was meticulously pipetted and utilized for further analysis.

2.4. Characterization of the GCN nanoparticles

The imaging of GCN nanoparticles was performed using an Apreo S high-resolution field-emission scanning electron microscopy (SEM) (Thermo Scientific Inc., Eindhoven, The Netherlands) at 2 kV. Before imaging, the nanoparticle dispersion in ethanol (EtOH) was drop-cast onto a polished, conductive silicon (Si) substrate and allowed to dry before analysis. X-ray diffraction (XRD) measurements were performed using a Panalytical Empyrean diffractometer which is outfitted with a five-axis goniometer and an Empyrean Cu LFF X-ray tube. The X-rays were filtered by a BraggHD monochromator. The absorbance spectrum was studied using a Jasco V-770 spectrophotometer, examining ethanolic dispersions of nanoparticles at a scan rate of 1000 nm/min with 0.5 nm intervals, spanning from 200 to 1400 nm. The Fourier-transform infrared (FTIR) spectra of the nanoparticle powder were acquired using an Invenio R spectrometer (Bruker Optics GmbH, Ettlingen, Germany) fitted with an attenuated total reflectance (ATR) crystal.

2.5. Cells and cell culture

GBM cell lines, LN229 and SNB19 (provided by Dr. Kirsi Granberg, Faculty of Medicine and Health Technology, Tampere University, Finland) and non-cancerous cells, Mouse embryonal fibroblast cells (MEF, provided by Prof. Pasi Kallio, Faculty of Medicine and Health Technology, Tampere University, Finland) were used for the *in vitro* analysis. These cell lines were grown in Dulbecco's Modified Eagle Medium (DMEM) enriched with 10 % fetal bovine serum (FBS), 0.1 mg/mL Streptomycin and 100 U/mL Penicillin. The cells were cultured at 37 °C in a humidified incubator with 5 % CO_2. All the culture media and antibiotics were obtained from Sigma-Aldrich, St. Louis, MO, United States.

2.6. Cytotoxicity effect of GCN-Np using MTT assay

Cytotoxicity effect of a new synthesized GCN nanoparticles on GBM cell lines was evaluated using MTT assay (AR1156-1, BOSTER, Pleasanton, CA, USA) (Palanivel et al., 2020). MEF cell lines were used as a control. Briefly, 5 x 10^3 cells/well of LN229, SNB19 and MEF cells were seeded in 96-well sterile plate and incubated at 37 °C for 24 h. A dose of 5 μg/mL GCN-Np has been shown to induce significant apoptosis-mediated cell death in hematological malignancies by increasing oxidative stress and intracellular levels of reactive oxygen species, leading to mitochondrial dysfunction (Liu et al., 2020; Martel-Estrada et al., 2025). Hence, this particular concentration was chosen for preliminary cytotoxic evaluation. Previous evidence demonstrates that a 5 μg/mL concentration of TMZ significantly enhances cell growth inhibition in GBM cells, therefore, this concentration was chosen in the preliminary screening to investigate the cytotoxic effects (Kaina et al., 2020; Kaina et al., 2020). Once the confluency reached to 60–70 %, the cells were treated with 5 μg/mL of GCN-Np and/or TMZ as a reference compound and 0.1 % DMSO as negative control and further incubated in cell culture environment for 48 h. Then, the growth medium was replaced with 100 μL of medium containing 10 μL of MTT solution and added to each well and incubated further for 2 h. The MTT-medium was aspirated to dissolve the formazan crystals in 100 μL of DMSO and incubated for 30 more minutes. The absorbance was measured using the microplate reader (SPARK®, TECAN, Mannedorf, Switzerland) at 450

nm and the % of cell growth inhibition with reference to the negative control was calculated using equation (1) The percentage of

$$Inhibition\ (\%) = 100 - \left(\frac{Absorbance\ treated\ cells}{Absorbance\ untreated\ cells\ (DMSO\ control)} x100\right) - - \rightarrow Eq. \quad (1)$$

2.7. Inhibitory kinetics of GCN-Np using trypan blue assay

The GCN-Np was further assessed for its inhibitory kinetics using a series of concentrations including 1 μg, 5 μg, 10 μg, 25 μg, and 50 μg. TMZ was used as a reference compound and DMSO was used as a negative control, LN229 and SNB19 wells were seeded at a density of 5 x 10^3 cells/well in 96-well sterile plate and cultured in appropriate cell culture environment. Briefly, at 60–70 % confluency, the cells were treated with the above-mentioned concentration of GCN-Np and TMZ for 48 h. The treated cells were trypsinized and centrifuged at 3000 rpm for 5 min and the cells were stained with trypan blue stain. The percentage of live and dead cells was quantified using Countess II FL, and the percentage inhibition of cell growth was calculated using equation (1) to normalize the data against the vehicle control DMSO. The dose-responsive curve was plotted from which the half maximal inhibitory concentration (IC_{50}) was calculated specifically for each cell and the compounds. The IC_{50} of the experimental set was ascertained utilizing a non-linear regression curve fitting model from GraphPad Prism 10, in accordance with the software's guidelines. Similarly, time-dependent analysis was also assessed to check the effect of GCN-Np on different cell lines at varying time points, 24 h and 48 h, following the above-mentioned protocol.

2.8. Effect of GCN-Np in cell cycle analysis

Cell cycle analysis was performed by staining the GCN-Np treated GBM cells with propidium iodide (PI) followed by FACS cytometric measurements. Briefly, the LN229 and SNB19 cells were cultured in 12 well culture dish at a density of 2 x 10^5 cells/well. Upon reaching confluency, GBM cells were treated with the IC_{50} concentrations of 3.9 μg/mL for LN229 and 10.7 μg/mL for SNB19 cell lines for 48 h. The cells were rinsed with 1X Phosphate buffered saline (PBS), fixed with 1 % ice-cold ethanol for 30 min, and thereafter utilized for FACS analysis. Prior to performing flow cytometry, the cells were stained with 50 μL of PI (1 mg/mL) in RNase1 (0.2 mg/ml) and incubated for 40 min at ambient temperature. The percentage of cells in each phase of the cell cycle was assessed using flow cytometry (CUBE 8, SYSMEX, Kobe, Japan) using FL2 channel at an excitation wavelength of 488 nm. Data analysis was conducted for 10000 cells/group using FlowJo version 10.8.1 (Coppard et al., 2024).

2.9. Role of GCN-Np in apoptosis and necrosis

Dual staining of GCN-Np treated GBM cells was performed using Acridine Orange (AO) and Ethidium Bromide (EB) to differentiate apoptosis from necrotic cell death (Lieger et al., 1995). AO/EB staining facilitates the identification of apoptosis-related changes in the cell membrane. The overall cell density, culture conditions, IC_{50} concentrations of cell line-specific for GCN-Np and TMZ, and the treatment period were similar to the cell cycle analysis. AO and EB were dissolved in DPBS at concentrations of 0.1 μM and 0.25 μM, respectively. Staining was performed at ambient temperature according to the manufacturer's protocol, followed by two washes in PBS to remove the excess stains, and the cells were subsequently extracted for flow cytometry analysis. The cells undergoing transitioning from apoptosis to necrosis were quantified using an excitation wavelength of 488 nm, with the emission detection filters set at 525/20 nm (FL1) and 635/20 nm (FL3). Data analysis was conducted for 10000 cells/group using FlowJo version 10.8.1.

2.10. Ability of GCN-Np in inducing reactive oxygen species in GBM cells

The formation of ROS production was assessed using employing 2′,7′-dichlorodihydrofluorescein diacetate (H2DCFDA) (Sigma-Aldrich, St. Louis, MO, United States), which remains non-fluorescent until oxidized by the presence of intracellular ROS. GBM cells were cultured in 12-well plates at a density of 2 x 10^5 cells/well to achieve 60–70 % confluency. The cells were subsequently treated with the IC_{50} concentration of GCN-Np and TMZ for 48 h 0.1 % DMSO served as a negative control whereas cells treated with hydrogen peroxide (200 μM) served as a reference compound. The cells were then resuspended and incubated in 20 μM 2′,7′-dichlorodihydrofluorescein diacetate (H2DCFDA) for 30 min. Further, cells were washed twice with DPBS, and seeded in 96-well black clear-bottom plate for fluorescence measurement using a microplate reader (SPARK®, TECAN, Mannedorf, Switzerland) at an excitation wavelength of 485 nm excitation and an emission wavelength of 535 nm. The changes in the fold level of ROS were calculated using equation (2).

$$FOLD\ change = \frac{Fluorescence\ treated\ cells - Fluorescence\ blank}{Fluorescence\ untreated\ cells\ (DMSO\ control) - Fluorescence\ blank} - - - \rightarrow Eq. \quad (2)$$

2.11. Cell death analysis for GCN-Np by mitochondrial membrane potential assay

The mitochondrial membrane potential (ΔΨm) was assessed using JC-10 kit based on the red-green fluorescence ratio. LN229 and SNB19 cells were seeded in a 96-well plate at a density of 3 x 10^4 cells/well. At 60–70 % confluency, the cells were treated with the IC_{50} of GCN-Np and TMZ (reference compound) and incubated for 48 h. After incubation, the cells were rinsed with DPBS, followed by the addition of 10 μL of (5,5,6,6′-tetrachloro-1,1′,3,3′ tetraethylbenzimi-dazoylcarbocyanine iodide) JC-10 dye (5 μg/mL). The complete mixture was incubated for 30 min, aspirated, and washed twice with DPBS before measuring the fluorescence in a microplate reader (SPARK®, TECAN, Mannedorf, Switzerland). Fluorescence emission was performed using a filter set to

excitation/emission wavelengths of 490/525 nm and 590 nm. The proportionality of red fluorescence (polarized) and green fluorescence (depolarized) in each treatment group was compared against the negative control DMSO, and the results were recorded as a percentage of cells.

2.12. Ability of GCN-Np in influencing the migration of GBM cells

The wound healing assay was conducted to assess the GCN-Np role in inhibiting the metastatic characteristics of LN229 and SNB19 cells. Cells were grown in 12- well plate at a density of 3.5 x 10^5 cells/well, until a confluent cell monolayer was formed in each well. Wounds were inflicted to each cell monolayer using a sterile pipette tip from edge to edge. The medium was thereafter removed, and the monolayers were rinsed with PBS to remove the floating cells. The cells were then treated with IC_{50} of GCN-Np and TMZ (reference compound), while DMSO served as the negative control. The wound healing area was viewed and calculated using equation (3) for every 1 h up to 5 h with microscopic images acquired using a light microscope at 4x magnification.

$$\text{Wchange}\ (\%) = \frac{W0 - D - W_{t-D}}{W0 - C - Wt - C} x\,100 \qquad \text{Eq. (3)}$$

where, W_{0-D} is the scratch area at starting point (0 h), W_{t-D} is the scratch area in GCN-Np and TMZ treated cells after 1–5 h, $W_{0\text{-}C}$ is the scratch area in DMSO treated sample at the 0 h, and $W_{t\text{-}C}$ is the scratch area in DMSO groups after 1–5 h incubation.

2.13. Statistical analysis

In all the experiments, the values are reported as mean ± standard deviation (SD) from at least n = 5 independent measurements. Two-way analysis of variance (ANOVA), followed by Sidak's multiple comparisons test and Tukey's multiple comparisons tests, was employed to statistically assess the acquired values, with significance threshold probabilities of *p-value <0.05, * *p < 0.001.

3. Results

3.1. GCN-Np preparation and characterization

Mechanical milling is an efficient and eco-friendly method for reducing the size and dimensions of bulk materials, facilitating the fabrication of particles ranging from nano-to micro-scales, leading to increased nanoparticle's activity. In the present work, GCN nanoparticles were synthesized using solvent-assisted grinding of bulk GCN in the ethanol. As the solvent's polarity increases, the yield of the synthesized nanoparticles improves. Scanning electron microscopy (SEM) (Fig. 1a) represents the morphology of the resultant GCN nanoparticles after the mechano-grinding process. The size of the GCN nanoparticles were determined to possess irregular shapes. The size distribution was established by measuring the longest dimension of 400 individual particles, resulting an average particle size of around 300 nm (**inset of** Fig. 1a). **T**he optical properties of the GCN nanoparticles were evaluated

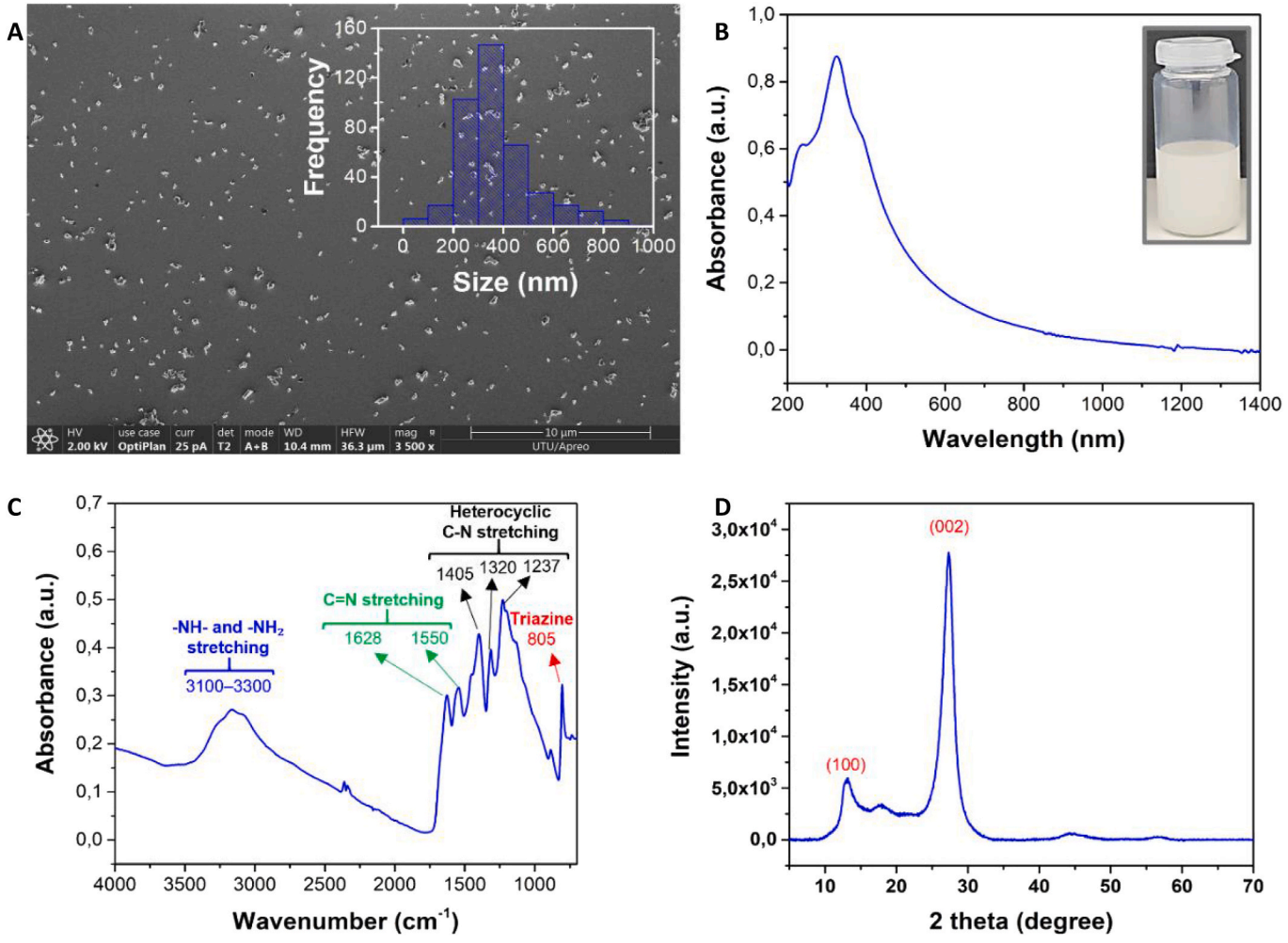

Fig. 1. Characterizations of (a) FE-SEM micrograph of GCN nanoparticles (inset: particle size distribution), (b) UV–VIS–NIR absorbance spectrum (inset: GCN nanoparticles dispersion), (c) FTIR spectrum, and (d) XRD diffraction pattern.

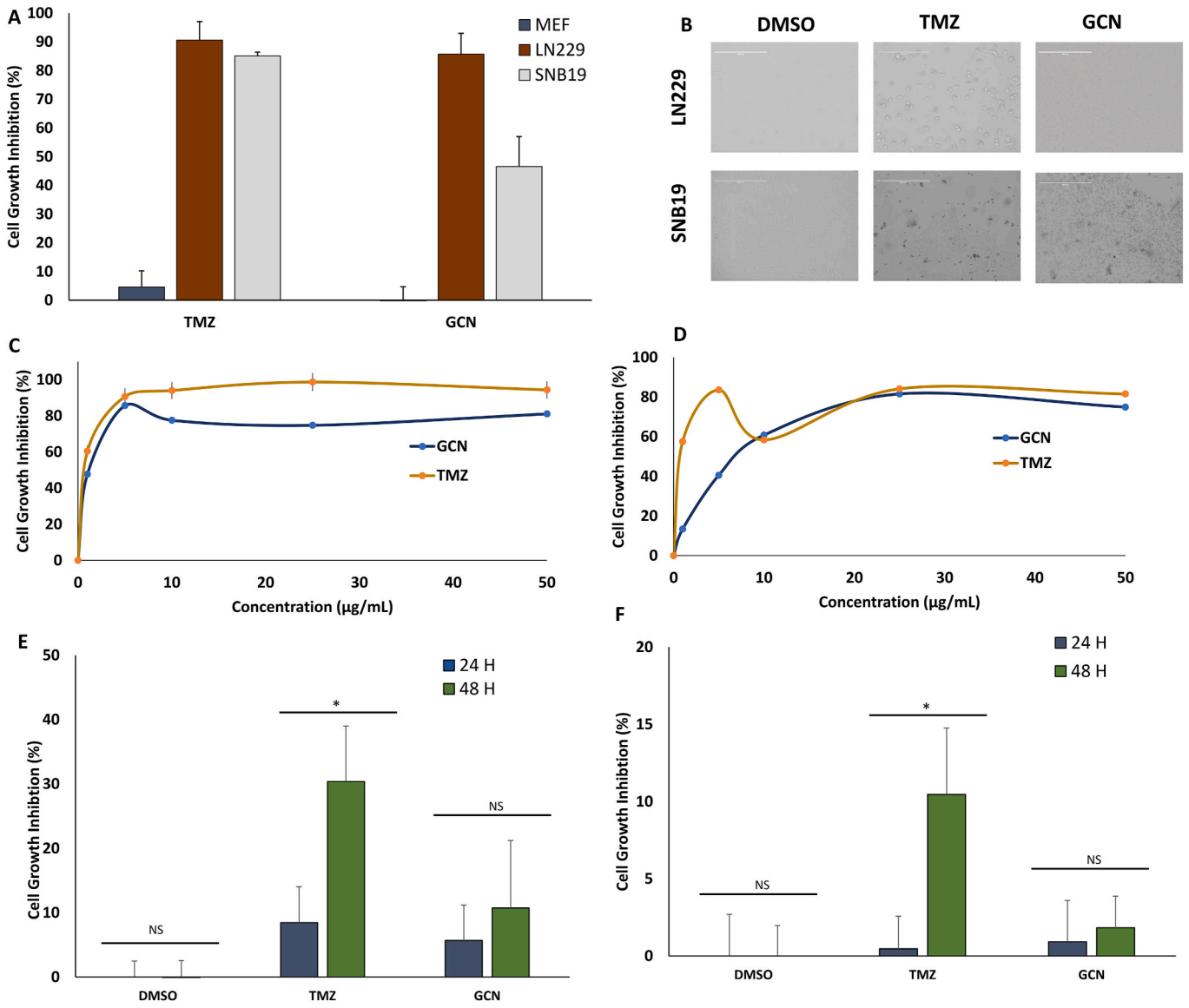

Fig. 2. Cell growth inhibition (%) of GCN-Np treated GBM cells: (A) MTT assay in LN229 and SNB19 cells, where MEF cells was used as a control using 5 µg/mL for 48 h; **(B)** Phase contrast microscopic images of GCN nanoparticle-. TMZ-treated LN229 and SNB19 cells with DMSO as a control. Dose-responsive assay with varying concentrations of GCN nanoparticles and TMZ, 1 µg, 5 µg, 10 µg, 25 µg, and 50 µg in **(C)** LN229 **(D)** SNB19 cells using trypan blue assay; Time-series analysis using the IC_{50} concentrations to assess the effect of GCN nanoparticles and TMZ in **(E)** LN229 cells **(F)** SNB19 cells, for 24 and 48 h where DMSO served as a negative control. All data was normalized against DMSO and represented as mean ± standard deviation (SD) with n = 5 independent values and was statistically analyzed by two-way analysis of variance (ANOVA) followed by Sidak's multiple comparisons test; Asterisk represents statistically significant data between GCN and TMZ, *$p < 0.05$, **$p < 0.001$., ns represents non-significant data. (For interpretation of the references to color in this figure legend, the reader is referred to the Web version of this article.)

using absorbance spectroscopy, which indicated a strong absorption peak in the UV region at ~325 nm, accompanied by an absorption tail extending into the visible region (Fig. 1b). Also, a colloidally stable GCN-Np suspension in ethanol was observed, as shown in the **inset of** Fig. 1b, confirming the distribution of smaller particle size, as verified earlier by SEM analysis.

Further, FT-IR spectroscopy elucidated the chemical bonding and vibrational modes of the GCN nanoparticles, where absorption peak at 805 cm^{-1} corresponding to the characteristic breathing mode of triazine units; peaks near 1550 cm^{-1} and 1628 cm^{-1} are attributed to C=N stretching, while bands at 1237 cm^{-1}, 1320 cm^{-1}, and 1405 cm^{-1} correspond to the stretching modes of C–N heterocycles. The broad absorption band at 3100–3300 cm^{-1} is assigned to the stretching modes of -NH- and -NH_2 functional groups (Fig. 1c). X-ray diffraction (XRD) analysis validated the structural properties of the GCN nanoparticles, with the (002) diffraction peak at approximately 27.4° signifying the distinctive interlayer stacking structure. The (100) diffraction peak at ~13° indicates the interplanar structural arrangements, hence confirming the successful fabrication of GCN nanoparticles (Fig. 1d). Thus, the synthesized GCN nanoparticles size is preferentially smaller in size than the GBM cell lines, LN229 and SNB19 selected for further studies, rendering them appropriate for cytotoxicity studies.

3.2. *Cytotoxicity activity of GCN nanoparticles on GBM cell lines*

Anticancer activity of GCN-Np was assessed by evaluating its cytotoxicity through the MTT assay in GBM cells. The % of cell growth inhibition for GCN-Np treated LN229 cells was 85 % with 90.5 % in TMZ treatment. GCN nanoparticles reduced the cell growth to 46.5 % in SNB19 cells with 85.5 % in TMZ treatment. Furthermore, TMZ was

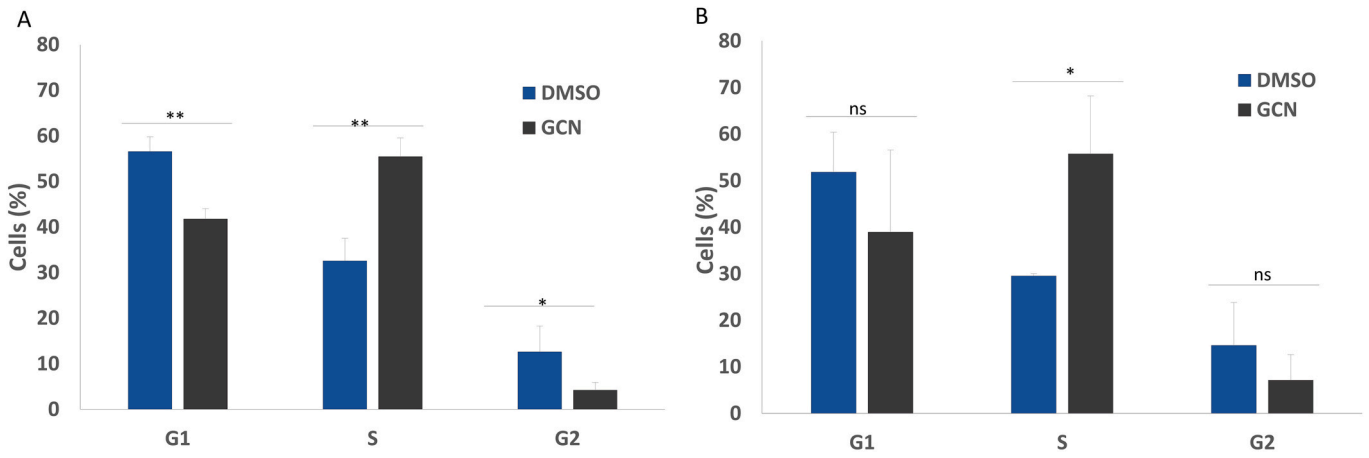

Fig. 3. Effects of GCN nanoparticles in the cell cycle of GBM cell lines. *Percentage of the total number of cells in different phases of the cell cycle after 48 h of treatment with GCN-Np and DMSO in LN229* ***(A)*** *and SNB19* ***(B)*** ***by*** *PI staining and flow cytometry. The results are shown as mean (n = 5) ± S.D and the statistical analysis was performed using one-way ANOVA followed by Sidak's multiple comparisons test. The asterisk represents significant differences between the treatment groups with the * p < 0.05; ns represents non-significance between treatment groups.*

found to significantly inhibit MEF cell growth by 4.6 %, whereas GCN-Np caused a 0.3 % increase in MEF cell growth (Fig. 2A). Fig. 2B showed the phase contrast microscopic images of GCN-Np and TMZ treated LN229 and SNB19 cells illustrating visible cell death, while DMSO as a control exhibiting live cells. A dose-responsive curve was performed to determine the IC_{50} concentration with varying concentrations 5 μg, 10 μg, 25 μg, and 50 μg. It was found that IC_{50} of GCN-Np treated LN229 cells was 3.9 μg/mL which was significantly lower than SNB19 with 10.7 μg/mL (Fig. 2C). TMZ-treated LN229 and SNB19 cells has exhibited higher IC_{50} values than GCN nanoparticles, which was 9.3

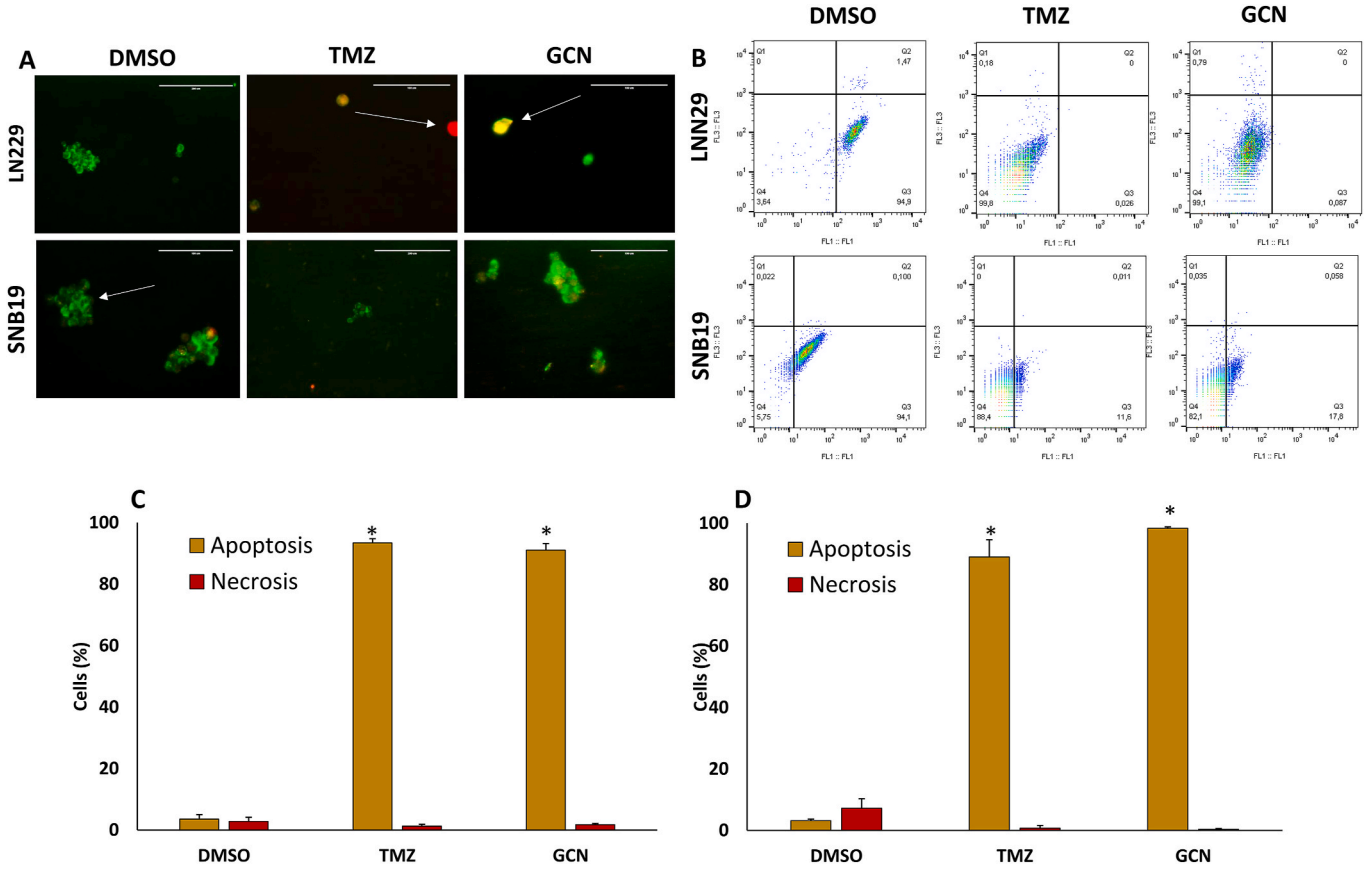

Fig. 4. Effects of GCN nanoparticles in inducing apoptosis in GBM cells: determined with an AO/EB dual staining. (A) Fluorescence microscopy images of LN229 and SNB19 cells lines, treated with the IC_{50} of GCN-Np and TMZ. Images were captured after 48 h of treatment; arrows indicate live cells (green), apoptotic cells (yellow) and necrotic cells (red); (B) Scatterplot from flow cytometry after gating the GBM cell population for live (Q3), apoptotic (Q4) and necrotic (Q1) cells after 48 h of treatment with GCN nanoparticle, TMZ and DMSO (control). Bar graphs representing the percentage of live, apoptotic, and necrotic cells in (C) LN229 and (D) SNB19 cells after 48 h of treatment. The asterisk represents statistically significant differences between the TMZ and GCN-Np treatments with * $p < 0.05$. All results are shown as mean (n = 5) ± S.D. (For interpretation of the references to color in this figure legend, the reader is referred to the Web version of this article.)

μg/mL and 16.8 μg/mL respectively (Fig. 2D). Time-dependent assessment at two distinct time points (24hr and 48 h) demonstrated a similar trend in the % of inhibition across both the cell lines. TMZ-treatment resulted in 30 % and 40 % inhibition in LN229 (Fig. 2E) and SNB19 cells (Fig. 2F), respectively, while GCN-Np treatment exhibited lower inhibition percentages of 10 % and 1.8 % at 48 h, respectively.

3.3. Effect of GCN nanaoparticles on cell cycle of GBM cells

Propidium idodide staining was performed to investigate the effect of GCN nanoparticles on cell cycle arrest, using the IC_{50} concentrations pertinent to the cell lines. DMSO was used as a control. GCN-Npexposure on LN229 cells reduced the cell population in G1 phase, with a significant arrest in S phase to approximately 55.5 % as compared to the DMSO control (32.5 %) (Fig. 3A). A similar tendency was noted in SNB19 cells, exhibiting a considerable S phase arrest compared to DMSO (29 %) (Fig. 3B). These results indicate that GCN nanoparticles has the ability to halt cell division prior to the initiation of DNA synthesis, hence preventing the GBM cell proliferation. Clinically, DNA damage-inducing drugs are highly valuable for cancer treatment, functioning through the direct or indirect creation of DNA lesions and the subsequent suppression of cellular growth. In addition to classical drugs like TMZ, there is a necessity for additional possible drugs that can induce DNA damage. Our findings indicates that GCN-Np could possibly inhibit DNA synthesis by introducing a novel class of GCN-based nanoparticle for GBM treatment.

3.4. GCN-Np induces apoptosis in GBM cell lines

Investigating apoptosis and necrosis is essential in evaluating anticancer drugs as both mechanisms signify different types of programmed cell death a cancer cells can bypass or utilize, hence influencing therapy efficacy and resistance. Thus, the effect of GCN-Np and TMZ was examined for the induction of apoptosis, a regulated cell death or necrosis, a nonregulated cell death in GBM cells by FACS. TMZ and DMSO were used as positive and negative controls, respectively. Treated cells stained with AO/EB were visualized under fluorescence microscope, with green-stained cells indicating live cells, yellow-stained cells denoting early apoptotic cells containing condensed or fragmented chromatin, and red/stained cells signifying necrosis or late apoptotic cells containing condensed and fragmented orange chromatin (Fig. 4A). The scatter plot obtained after gating (Fig. 4B) illustrates the variations in cells size, heterogeneity, and proportion of each cell in different stages of cell death. Based on the FACS analysis, GCN-Np and TMZ treated-LN229 cells displayed 91 % and 93 % of apoptotic cells respectively (Fig. 4C). Likewise, SNB19-treated cells exhibited a significant presence of 8 % of cells in GCN-Np treated cells, compared to 89 % of cells in TMZ-treated SNB19 cells (Fig. 4D). Overall, <10 % of necrotic cells were observed in both the GCN-Np and TMZ-treated cell lines. Also, DMSO-treated control cells exhibit the lowest level of apoptotic and necrotic cells.

3.5. GCN nanoparticles depolarizes the mitochondrial membrane integrity in GBM cells due to ROS production

Depolarization of the mitochondrial membrane is a characteristic feature of apoptosis, potentially resulting from the release of reactive oxygen species and/or many apoptotic proteins. The permeability of the mitochondrial membrane (ΔΨm) is an important indicator of mitochondrial activity and acts as a measure of intact cell. JC-10 dye accumulates in healthy mitochondria resulting in the formation of reversible red-fluorescent JC-10 aggregates (Ex/Em = 540/590 nm). In apoptotic cells, the mitochondrial membrane potential decreases, leading to the inability to retain JC-10 dye, which returns to its monomeric green form (EX/Em = 490/525 nm) in the cytosol. The specified ratio is determined by dividing the fluorescence at 525 nm (green) by the fluorescence at 590 nm (red). To elucidate the mitochondrial involvement in the GCN-Np-induced apoptotic process, alterations in the ΔΨm was assessed in the GBM cell lines using JC-10 dye. Typically, in normal cells, the JC-10 dye concentrates in the mitochondrial matrix, producing red fluorescence color, however when there is a dissipation of ΔΨm, the dye disperses throughout the cell, leading to a shift from red to green fluorescence. A reduced MMP indicates diminished red fluorescence, resulting in a higher ratio compared to the control cells. Here, GCN-Np treated LN229 cells exhibited an increased red/green fluorescence ratio of about 25 %, in contrast to 15 % observed in TMZ relative to the DMSO control. Simultaneously, the ratio in GCN treated SNB19 cells decreased by 5 %, while the ratio in TMZ increased to 35 % (Fig. 5A). Our results indicated that GCN-Np generated a higher red to green ratio in LN229 compared to SNB19 significantly affecting ΔΨm, which reflects cell-line specific depolarization and apoptosis induction. This ΔΨm depolarization may result from the ability of the GCN-Np and TMZ in disrupting the

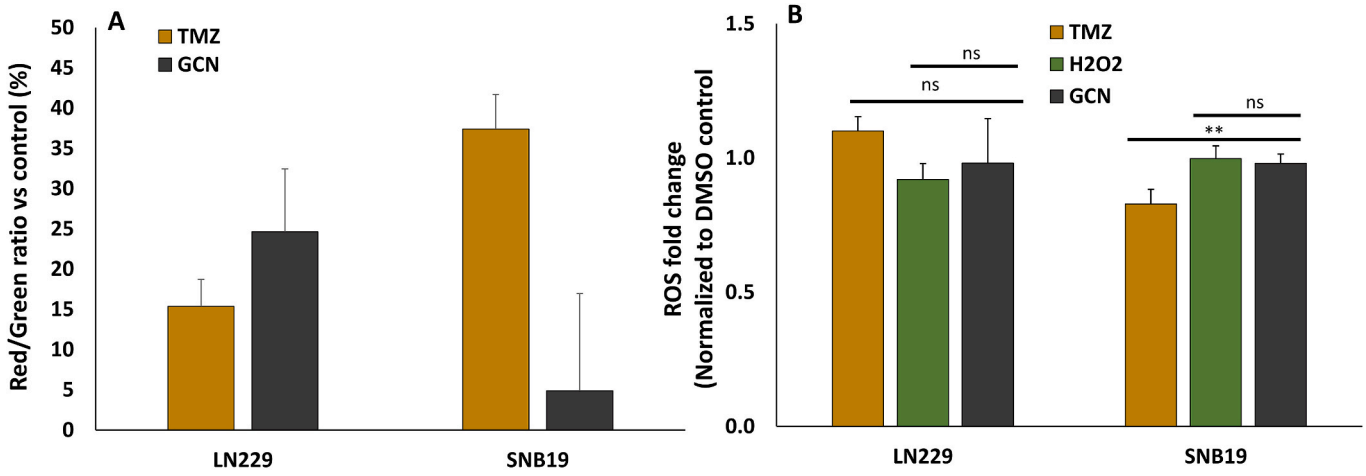

Fig. 5. Effects on the mitochondrial membrane potential (ΔΨm) and intracellular ROS (iROS) in GBM cell lines. (A) Red/green fluorescence ratio in the GBM cell lines, LN229 and SNB19 after 48 h treatment with IC_{50} concentration of GCN-Np and TMZ; **(B)** Fold change in the intracellular ROS (iROS) levels in LN229 and SNB19 cells upon treatment with IC_{50} concentration of GCN nanoparticle, TMZ and H_2O_2 for 48 h using H2DCFDA. All data was normalized against DMSO. Asterisk represents statistically significant data between GCN-Np and TMZ, using one-way ANOVA with turkey multiple comparison test for ROS; *$p < 0.05$, **$p < 0.001$. ns represents non-significant data between GCN-Np and H_2O_2. (For interpretation of the references to color in this figure legend, the reader is referred to the Web version of this article.)

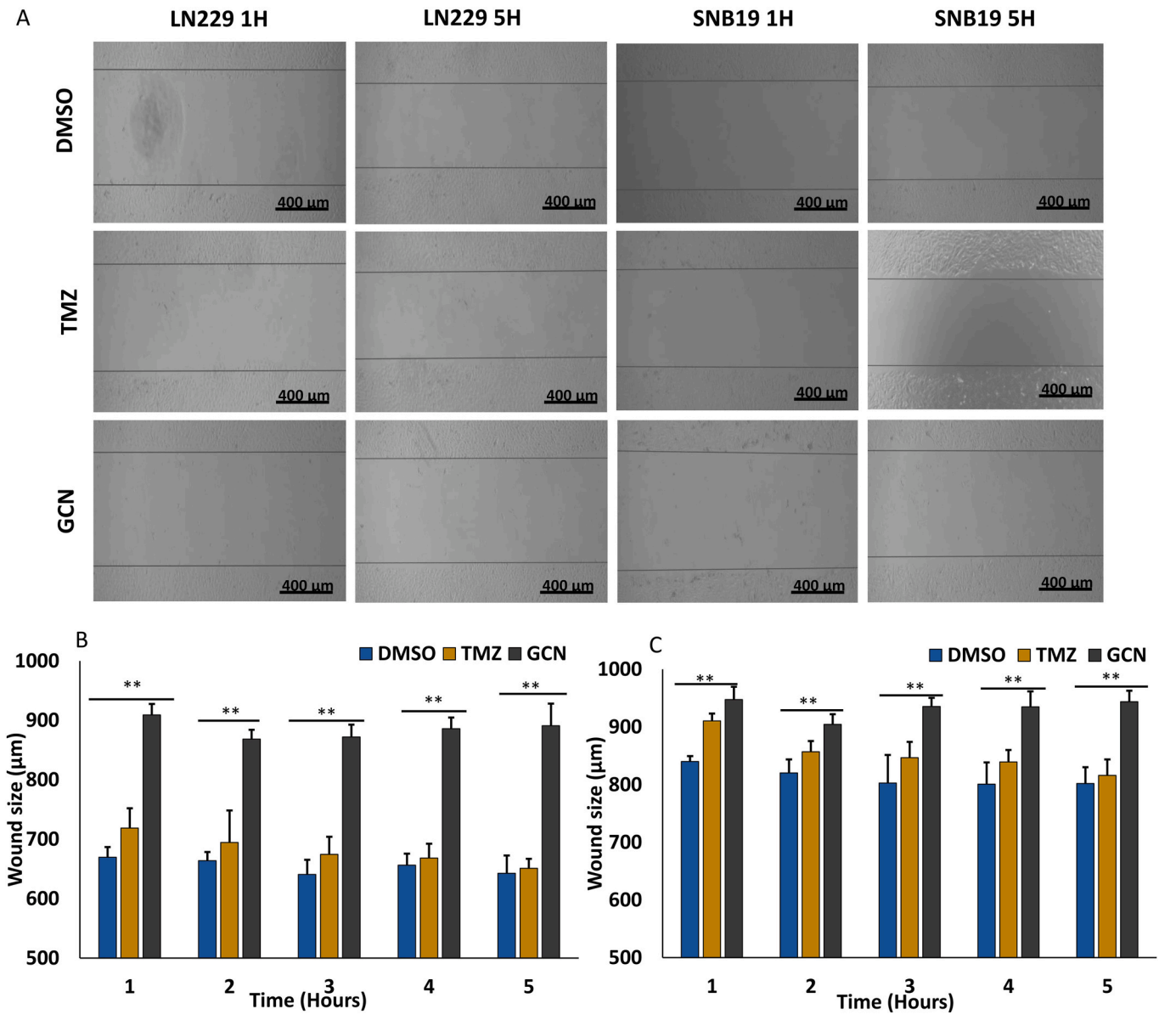

Fig. 6. Migration inhibition of GBM cells treated with GCN nanoparticles. (A) Microscopic images illustrating the migration of LN229 and SNB19 cells after treatment with IC_{50} concentration of GCN, TMZ and DMSO for different time intervals, 0hr, 1hr, 2 h, 3 h,4 h & 5 h using scratch assay. Bar diagram representing the wound size (µm) after treatment with IC_{50} concentration of GCN, TMZ and DMSO for LN229 (B) and SNB19 (C). Results were represented as a mean ± S.D with a n = 5 and the statistical analysis was performed using one-way ANOVA followed by Sidak's multiple comparisons test. Asterisks represents significant difference between Control and GCN, respectively. */+ $p < 0.05$ and **/++ $p < 0.001$. ns represents non-significant differences.

internal environment of the GBM cells by ROS. Thus, ROS was evaluated in the GBM cells with H_2O_2 as a control. TMZ treated-LN229 cells exhibited 1.1-fold rise in the ROS production, while GCN treated LN229 cells displayed a 0.98-fold increase in ROS level. TMZ treated-SNB19 cells exhibited a 0.83-fold increase, but GCN nanoparticle-treated SNB19 cells demonstrated an increase of 0.98-fold (Fig. 5B). All results were normalized against the DMSO control. Thus, it was observed in both the cell lines, ROS production was equal to H_2O_2 upon treatment with GCN-Np and TMZ, which confirms their potential to induce ROS-mediated apoptosis.

3.6. GCN nanoparticles interfere with the cell motility of the GBM cells

GBM cells represent a highly invasive form of cancer, therefore, understanding the impact of GCN-Np on the chemotactic mobility of those cells is of significant interest. In the wound healing experiment, we investigated cell migration following a mechanically induced scratch in the presence of IC_{50} concentration of GCN-Np and TMZ in both LN229 and SNB19 cell lines. Fig. 6A presents the 4x microscopic images of the DMSO control, GCN-Np, and TMZ treated GBM cell lines illustrating the closure of the scratch at various time intervals, 0 h, 1 h, 2 h, 3 h, 4 h, and 5 h. Our data clearly shows that treatment with GCN-Np in LN229 and SNB19 cells caused a significant inhibition of cell migration in a time-dependent manner than the TMZ and DMSO control (Fig. 6B & C). Overall, the data revealed that GCN may potentially inhibit the migration of the GBM cells, hence preventing the re-establishment of cell-cell contact that promotes GBM cell proliferation.

4. Discussion

Glioblastoma, an aggressive and deadly brain cancer, needs a comprehensive understanding of the various available therapeutic

approaches for successful treatment. The chemotherapeutic drugs that are currently available including carmustine, procarbazine, lomustine, and temozolamide, are limited in their effectiveness due to their instability, inadequate pharmacokinetics, off-target toxicity, and rapid clearance in physiological settings (Ortiz et al., 2021). Nanoparticles are extensively used as a novel treatment approach in the contemporary medical field. (g-C_3N_4), an excellent drug carrier is obtainable in 0–3 dimensions as nanopowders, nanoparticles, nanogels, nanosheets, nanotubes, nanoquantum, and naodots. In recent years, nanoparticles measuring 100–200 nm in size have been designed to enhance the accumulation in the tumor region with higher retention time (Etter et al., 2021). The current investigation revealed that the average particle size of GCN-Np produced via mechanical grinding was approximately 300 nm, which was notably larger than the GBM cells being examined, measuring 12–14 μm (Li et al., 2015). As observed by (Jiang et al., 2014), the FTIR analysis revealed the spectral area at distinct regions which were attributed to the presence of functional groups of g-C_3N_4: C=N stretching at 1550 cm^{-1} and 1628 cm^{-}, of C–N heterocycles at 1237 cm^{-1}, 1320 cm^{-1}, and 1405 cm^{-1}; and -NH- and -NH_2 functional groups at 3100–3300 cm^{-1} peaks.

Graphitic carbon nitride demonstrated therapeutic potential against many cancer cell lines, including glioblastoma, lung, liver, ovarian carcinoma, breast, skin, and glioma cells (Atia et al., 2022; Godwin et al., 2019; Padervand et al., 2022). Previous studies on GCN nanoparticles have demonstrated its cytotoxicity effect targeting cancerous cells (Chan et al., 2016; Heo et al., 2018; Liu et al., 2018; Taheri et al., 2020; Yadav et al., 2022). We found that GCN induces cell growth inhibition in LN229 by around 85 % compared to 46.5 % inhibition in SNB19, demonstrating its efficacy comparable to temozolomide. The disparity in the cell growth inhibition between LN229 and SNB19 cells may be attributed to cell-line specificity. GCN-Np also showed <1 % growth inhibition in normal cells, specifically MEF, indicating its potential as an anti-cancerous drug.

Graphitic carbon nitride combined with curcumin demonstrated excellent drug release, inducing apoptosis against MCF-7 breast cancer cells (Abdouss et al., 2023), with the underlying mechanism being the generation of ROS production (Saumya et al., 2023). Similarly, Zn NPs/g-C_3N_4 NS generated free radicals, resulting in the generation of ROS which distributed the mitochondrial membrane potential, and ultimately caused cell death (Leelavathi et al., 2022). In the present study, the GCN nanoparticles produced an equal fold of ROS comparable to TMZ, thus inducing ROS-mediated apoptosis.

GBM dismal prognosis is attributed to its significant invasiveness (Hanif et al., 2017; Louis et al., 2016; McKinnon et al., 2021), resulting in metastasis and the recurrence of tumors immediately after treatment. A study performed by (Yoshihara et al., 2024) on g-C3N4 has demonstrated its capacity to inhibit cell migration in U87 glioblastoma cells. Consistent with the aforementioned report, our findings also demonstrated the prevention of cell migration in both LN229 and SNB19 cells compared to the existing chemotherapeutic agent, TMZ. Overall, our study has shown the GCN nanoparticle's anti-GBM effect comparable to TMZ, necessitating intensive molecular investigation to explore its therapeutic implications.

5. Conclusion

In summary, we have presented an overview of the synthesis and characterization of GCN nanoparticles through various analytical techniques. The present study revealed that GCN nanoparticles are a promising anti-GBM agent, as it affect the growth, proliferation and viability of LN229 and SNB19 cells. The findings indicate that the observed cytotoxic effect of GCN nanoparticles might be caused by an elevated ROS production and a shift in mitochondrial membrane potential. Furthermore, GCN-Np had the capability of inhibiting the mobility of GBM cells. In conclusion, the potential of GCN nanoparticles can be further structurally improved in size and functionally explored to be utilized as a therapeutic agent against GBM treatment. Further research warrants to determine the use of GCN-Np as a viable drug delivery system for GBM therapy.

CRediT authorship contribution statement

Anxo Vila Alonso: Writing – original draft, Visualization, Validation, Methodology, Formal analysis, Data curation. **Akshaya Murugesan:** Writing – review & editing, Writing – original draft, Validation, Formal analysis. **Rituporn Gogoi:** Writing – review & editing, Writing – original draft, Methodology, Investigation. **Sureka Chandrabose:** Visualization, Software. **Kasim S. Abass:** Writing – review & editing, Software. **Vipul Sharma:** Writing – review & editing, Writing – original draft, Visualization, Validation, Project administration, Funding acquisition, Formal analysis, Data curation. **Meenakshisundaram Kandhavelu:** Writing – review & editing, Writing – original draft, Project administration, Investigation, Conceptualization.

Declaration of competing interest

The authors declare no competing financial interest.

Acknowledgments

Authors are thankful to the Materials Research Infrastructure (MARI) and Sustainable Fabrication (SusFab) at the University of Turku for infrastructure facilities.

Data availability

Data will be made available on request.

References

Abdouss, H., Pourmadadi, M., Zahedi, P., Abdouss, M., Yazdian, F., Rahdar, A., Díez-Pascual, A.M., 2023. Green synthesis of chitosan/polyacrylic acid/graphitic carbon nitride nanocarrier as a potential pH-sensitive system for curcumin delivery to MCF-7 breast cancer cells. Int. J. Biol. Macromol. 242, 125134. https://doi.org/10.1016/j.ijbiomac.2023.125134.

Akhtar, M.J., Alhadlaq, H.A., Kumar, S., Alrokayan, S.A., Ahamed, M., 2015. Selective cancer-killing ability of metal-based nanoparticles: implications for cancer therapy. Arch. Toxicol. 89, 1895–1907. https://doi.org/10.1007/s00204-015-1570-1.

Alam, K.M., Kumar, P., Kar, P., Thakur, U.K., Zeng, S., Cui, K., Shankar, K., 2019. Enhanced charge separation in g-C3N4–BiOI heterostructures for visible light driven photoelectrochemical water splitting. Nanoscale Adv. 1, 1460–1471. https://doi.org/10.1039/C8NA00264A.

Anandasabapathy, S., Asirwa, C., Grover, S., Mungo, C., 2024. Cancer burden in low-income and middle-income countries. Nat. Rev. Cancer 24, 167–170. https://doi.org/10.1038/s41568-023-00659-2.

Anh Tran, T., Krishnamoorthy, K., Song, Y.W., Cho, S.K., Kim, S.J., 2014. Toxicity of nano molybdenum trioxide toward invasive breast cancer cells. ACS Appl. Mater. Interfaces 6, 2980–2986. https://doi.org/10.1021/am405586d.

Atia, Y.A., Bokov, D.O., Zinnatullovich, K.R., Kadhim, M.M., Suksatan, W., Abdelbasset, W.K., Hammoodi, H.A., Mustafa, Y.F., Cao, Y., 2022. The role of amino acid functionalization for improvement of adsorption thioguanine anticancer drugs on the boron nitride nanotubes for drug delivery. Mater. Chem. Phys. 278, 125664. https://doi.org/10.1016/j.matchemphys.2021.125664.

Chan, M.-H., Chen, C.-W., Lee, I.-J., Chan, Y.-C., Tu, D., Hsiao, M., Chen, C.-H., Chen, X., Liu, R.-S., 2016. Near-infrared light-mediated photodynamic therapy nanoplatform by the electrostatic assembly of upconversion nanoparticles with graphitic carbon nitride quantum dots. Inorg. Chem. 55, 10267–10277. https://doi.org/10.1021/acs.inorgchem.6b01522.

Cheng, J.-Z., Liu, L.-L., Liao, G., Shen, Z.-Q., Tan, Z.-R., Xing, Y.-Q., Li, X.-X., Yang, K., Chen, L., Liu, S.-Y., 2020. Achieving an unprecedented hydrogen evolution rate by solvent-exfoliated CPP-Based photocatalysts. J. Mater. Chem. A 8, 5890–5899. https://doi.org/10.1039/C9TA13514F.

Coppard, V., Szep, G., Georgieva, Z., Howlett, S.K., Jarvis, L.B., Rainbow, D.B., Suchanek, O., Needham, E.J., Mousa, H.S., Menon, D.K., Feyertag, F., Mahbubani, K. T., Saeb-Parsy, K., Jones, J.L., 2024. FlowAtlas: an interactive tool for high-dimensional immunophenotyping analysis bridging FlowJo with computational tools in julia. Front. Immunol. 15, 1425488. https://doi.org/10.3389/fimmu.2024.1425488.

Etter, E.L., Mei, K.-C., Nguyen, J., 2021. Delivering more for less: nanosized, minimal-carrier and pharmacoactive drug delivery systems. Adv. Drug Deliv. Rev. 179, 113994. https://doi.org/10.1016/j.addr.2021.113994.

Foo, C.Y., Fu, R.Z., 2021. Unravelling the potential of graphene in glioblastoma therapy. Mater. Sci. Eng., C 128, 112330. https://doi.org/10.1016/j.msec.2021.112330.
Fu, P.P., Xia, Q., Hwang, H.-M., Ray, P.C., Yu, H., 2014. Mechanisms of nanotoxicity: generation of reactive oxygen species. J. Food Drug Anal. 22, 64–75. https://doi.org/10.1016/j.jfda.2014.01.005.
Godwin, M.A., Mahithashri, K., Shiney, O.J., Bhagat, M., Praseetha, P.K., 2019. Metal incorporated g-C_3N_4 nanosheets as potential cytotoxic agents for promoting free radical scavenging in cancer cell lines. J. Nanosci. Nanotechnol. 19, 5448–5455. https://doi.org/10.1166/jnn.2019.16572.
Hanif, F., Muzaffar, K., Perveen, K., Malhi, S.M., Simjee, S., 2017. Glioblastoma multiforme: a review of its epidemiology and pathogenesis through clinical presentation and treatment. Asian Pac. J. Cancer Prev. APJCP : Asian Pac. J. Cancer Prev. APJCP 18, 3–9. https://doi.org/10.22034/APJCP.2017.18.1.3.
Heo, N.S., Lee, S.U., Rethinasabapathy, M., Lee, E.Z., Cho, H.-J., Oh, S.Y., Choe, S.R., Kim, Y., Hong, W.G., Krishnan, G., Hong, W.H., Jeon, T.-J., Jun, Y.-S., Kim, H.J., Huh, Y.S., 2018. Visible-light-driven dynamic cancer therapy and imaging using graphitic carbon nitride nanoparticles. Mater. Sci. Eng. C 90, 531–538. https://doi.org/10.1016/j.msec.2018.04.035.
Jiang, B., Fan, W., Sun, M.-Y., Ye, Q., Wang, S.-L., Tu, S.-J., Li, G., 2014. Domino reaction of arylglyoxals with Pyrazol-5-amines: selective access to pyrazolo-fused 1,7-Naphthyridines, 1,3-Diazocanes, and pyrroles. J. Org. Chem. 79, 5258–5268. https://doi.org/10.1021/jo500823z.
Kaina, B., Beltzig, L., Piee-Staffa, A., Haas, B., 2020. Cytotoxic and senolytic effects of methadone in combination with temozolomide in glioblastoma cells. Int. J. Mol. Sci. 21, 7006. https://doi.org/10.3390/ijms21197006.
Kim, C.-H., Lee, S.-Y., Rhee, K.Y., Park, S.-J., 2024. Carbon-based composites in biomedical applications: a comprehensive review of properties, applications, and future directions. Adv. Compos. Hybrid Mater. 7, 55. https://doi.org/10.1007/s42114-024-00846-1.
Leelavathi, H., Muralidharan, R., Abirami, N., Tamizharasan, S., Kumarasamy, A., Arulmozhi, R., 2022. Exploration of ZnO decorated g-C3N4 amphiphilic anticancer drugs for antiproliferative activity against human cervical cancer. J. Drug Deliv. Sci. Technol. 68, 103126. https://doi.org/10.1016/j.jddst.2022.103126.
Li, Q., Rycaj, K., Chen, X., Tang, D.G., 2015. Cancer stem cells and cell size: a causal link? Semin. Cancer Biol. 35, 191–199. https://doi.org/10.1016/j.semcancer.2015.07.002.
Lieger, Teri J., Hyun, Willian, Benedict Yen, T.S., Stites, Daniel P., 1995. Detection and quantification of live, apoptotic, and necrotic human peripheral lymphocytes by single-laser flow cytometry. Clin. Diagn. Lab. Immunol. 2, 369–376. https://doi.org/10.1128/cdli.2.3.369-376.1995.
Liu, C., Qin, H., Kang, L., Chen, Z., Wang, H., Qiu, H., Ren, J., Qu, X., 2018. Graphitic carbon nitride nanosheets as a multifunctional nanoplatform for photochemical internalization-enhanced photodynamic therapy. J. Mater. Chem. B 6, 7908–7915. https://doi.org/10.1039/C8TB02535E.
Liu, L., Zhang, M., Zhang, Q., Jiang, W., 2020. Graphene nanosheets damage the lysosomal and mitochondrial membranes and induce the apoptosis of RBL-2H3 cells. Sci. Total Environ. 734, 139229. https://doi.org/10.1016/j.scitotenv.2020.139229.
Louis, D.N., Perry, A., Reifenberger, G., von Deimling, A., Figarella-Branger, D., Cavenee, W.K., Ohgaki, H., Wiestler, O.D., Kleihues, P., Ellison, D.W., 2016. The 2016 world health organization classification of tumors of the central nervous system: a summary. Acta Neuropathol. 131, 803–820. https://doi.org/10.1007/s00401-016-1545-1.
Maiti, D., Tong, X., Mou, X., Yang, K., 2019. Carbon-based nanomaterials for biomedical applications: a recent study. Front. Pharmacol. 9. https://doi.org/10.3389/fphar.2018.01401.
Martel-Estrada, S.-A., Vargas-Requena, C.-L., Sifuentes-Chavarría, J.-I., Yepes-Mendoza, M.-Y., Palacio-Castillo, D.-S., Jimenez-Vega, F., Olivas-Armendáriz, I., 2025. Cell death mechanisms produced by carbon-based nanoparticles. J. Nanotechnol., 9961520 https://doi.org/10.1155/jnt/9961520, 2025.
Marucci, G., Lammi, C., Buccioni, M., Dal Ben, D., Lambertucci, C., Amantini, C., Santoni, G., Kandhavelu, M., Abbracchio, M.P., Lecca, D., Volpini, R., Cristalli, G., 2011. Comparison and optimization of transient transfection methods at human astrocytoma cell line 1321N1. Anal. Biochem. 414, 300–302. https://doi.org/10.1016/j.ab.2011.02.028.
McKinnon, C., Nandhabalan, M., Murray, S.A., Plaha, P., 2021. Glioblastoma: clinical presentation, diagnosis, and management. Br. Med. J. 374. https://doi.org/10.1136/bmj.n1560.
Ortiz, R., Perazzoli, G., Cabeza, L., Jiménez-Luna, C., Luque, R., Prados, J., Melguizo, C., 2021. Temozolomide: an updated overview of resistance mechanisms, nanotechnology advances and clinical applications. Curr. Neuropharmacol. 19, 513–537. https://doi.org/10.2174/1570159X18666200626204005.
Padervand, M., Nasiri, F., Hajiahmadi, S., Bargahi, A., Esmaeili, S., Amini, M., Karimi Nami, R., Shahsavari, Z., Karima, S., 2022. Ag@Ag2MoO4 decorated polyoxomolybdate/C3N4 nanostructures as highly efficient photocatalysts for the wastewater treatment and cancer cells killing under visible light. Inorg. Chem. Commun. 141, 109500. https://doi.org/10.1016/j.inoche.2022.109500.
Palanivel, S., Yli-Harja, O., Kandhavelu, M., 2020. Alkylamino phenol derivative induces apoptosis by inhibiting EGFR signaling pathway in breast cancer cells. Anti Cancer Agents Med. Chem. 20, 809–819. https://doi.org/10.2174/1871520620666200213101407.
Saleem, J., Wang, L., Chen, C., 2018. Carbon-based nanomaterials for cancer therapy via targeting tumor microenvironment. Adv. Healthcare Mater. 7, e1800525. https://doi.org/10.1002/adhm.201800525.
Saumya, Imtiyaz, K., Rizvi, M.A., Nenavathu, B.P., 2023. Fabrication of graphitic carbon nitride/barium hydroxide nanocomposite as an effective anticancer agent against MCF-7 cell lines. ChemistrySelect 8, e202301710. https://doi.org/10.1002/slct.202301710.
Taheri, H., Unal, M.A., Sevim, M., Gurcan, C., Ekim, O., Ceylan, A., Syrgiannis, Z., Christoforidis, K.C., Bosi, S., Ozgenç, O., Gómez, M.J., Turktas Erken, M., Soydal, Ç., Eroğlu, Z., Bitirim, C.V., Cagin, U., Arı, F., Ozen, A., Kuçuk, O., Delogu, L.G., Prato, M., Metin, Ö., Yilmazer, A., 2020. Photocatalytically active graphitic carbon nitride as an effective and safe 2D material for in vitro and in vivo photodynamic therapy. Small 16, e1904619. https://doi.org/10.1002/smll.201904619.
Wang, R.-C., Lin, Y.-C., Chen, H.-C., Lin, W.-Y., 2021. Energy harvesting from g-C3N4 piezoelectric nanogenerators. Nano Energy 83, 105743. https://doi.org/10.1016/j.nanoen.2021.105743.
Yadav, P., Mimansa, Kailasam, K., Shanavas, A., 2022. Nontoxic metal-free visible light-responsive carbon nitride quantum dots cause oxidative stress and cancer-specific membrane damage. ACS Appl. Bio Mater. 5, 1169–1178. https://doi.org/10.1021/acsabm.1c01219.
Yalamarty, S.S.K., Filipczak, N., Li, X., Subhan, M.A., Parveen, F., Ataide, J.A., Rajmalani, B.A., Torchilin, V.P., 2023. Mechanisms of resistance and current treatment options for glioblastoma multiforme (GBM). Cancers (Basel) 15. https://doi.org/10.3390/cancers15072116.
Yoshihara, N., Lopes, M., Santos, I., Kopke, B., Almeida, C., Araújo, J., Fechine, P.B.A., Santos-Oliveira, R., Sant'Anna, C., 2024. Graphitic carbon nitride as a novel anticancer agent: potential mechanisms and efficacy in prostate cancer and glioblastoma treatment. Biomater. Sci. 12, 5547–5561. https://doi.org/10.1039/D4BM01025F.
Zhang, Q., Liu, S., Zhang, Y., Zhu, A., Li, J., Du, X., 2016. Enhancement of the photocatalytic activity of g-C3N4 via treatment in dilute NaOH aqueous solution. Mater. Lett. 171. https://doi.org/10.1016/j.matlet.2016.02.043.